Simulations of the penetration of limestone targets using two dimensional multimodal fourier analysis

M. Brun, A. Combescure, C. Baillis, A. Limam, E. Buzaud

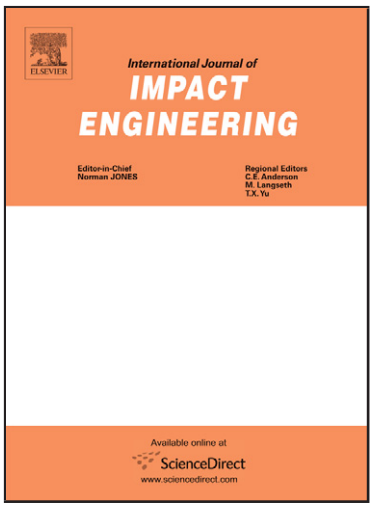

www.elsevier.com/locate/ijimpeng

Simulations of the penetration of limestone targets using two dimensional multimodal fourier analysis

M. Brun, A. Combescure, C. Baillis, A. Limam, E. Buzaud

PII: S0734-743X(07)00015-2
DOI: doi:10.1016/j.ijimpeng.2007.02.004
Reference: IE 1461

To appear in: *International Journal of Impact*

Received date: 10 December 2004
Revised date: 1 August 2006
Accepted date: 5 February 2007

Cite this article as: M. Brun, A. Combescure, C. Baillis, A. Limam and E. Buzaud, Simulations of the penetration of limestone targets using two dimensional multimodal fourier analysis, *International Journal of Impact* (2007), doi:10.1016/j.ijimpeng.2007.02.004

SIMULATIONS OF THE PENETRATION OF LIMESTONE TARGETS USING TWO DIMENSIONAL MULTIMODAL FOURIER ANALYSIS

M. BRUN[1,*], A. COMBESCURE[2], C. BAILLIS[2], A. LIMAM[1], E. BUZAUD[3]

[1]*Institut National des Sciences Appliquées de Lyon, 69621 Villeurbanne, France*

[2]*EC2-MS, 66 bd Niels BOHR, BP 2132 ,69603 VILLEURBANNE, France*

[3]*Centre d'Etudes de Gramat, 46500 Gramat, France*

Abstract

This paper is devoted to the presentation of a finite element based on a Fourier modal description of physical values on circumferences for a quasi-axisymmetric structure. The finite element detailed in this paper is an advanced version of the COMU element, developed by Combescure [1,2], in order to extend it for simulating penetration of targets composed of geological materials by steel projectiles. A finite element code with COMU elements is coupled with analytical forcing functions based on the dynamic expansion of a spherical cavity to represent the target. This combined analytical and computational approach is employed to reproduce normal impact of ogive-nosed VAR 4340 steel projectiles striking limestone targets with small angles of pitch and yaw. Results obtained from the cost-effective approach with two-dimensional COMU elements are checked against experimental data (Frew *et al*., [3]) and results from an analogous combined approach using three-dimensional hexahedral continuum elements (Warren, [4]).

Keywords : projectile impact, axisymmetric shell, non axisymmetric loading, multimodal Fourier analysis.

[*] Assistant Professor, corresponding author., Tel : 33-(0) 4-72-43-63-78, E-mail : Michael.Brun@insa-lyon.fr

1. INTRODUCTION

During the last two decades, analytical models for penetration mechanics have been intensively developed. Those application oriented tools are based on an approximation of the main physical processes implied in the interaction. In the case of a projectile striking a target, it is generally assumed that the projectile remains rigid during the penetration. The forces acting on the outer surface of the projectile during the penetration process can be estimated through empirical relations (Young [5]), or alternatively be derived from the resolution of a simplified problem. For instance, the solution of a dynamic spherical cavity expansion problem can be used as an input to the penetration equations, by assuming that the stress on the outer surface of projectile through penetration is determined by the stress on the surface cavity. This approach has been developed and adapted to several materials such as soil, concrete or limestone in Refs [6-9]. The dynamic cavity expansion problem is solved by considering appropriate constitutive laws for the target materials. Functional forms used for the target representation incorporate an unknown target resistance strength parameter that is obtained from penetration depth versus striking velocity data.

Fully three-dimensional penetration calculations with a purely computational approach (finite element method for both projectile and target in Lagrangian, Eulerian or Arbitrary Lagrangian-Eulerian formulations) enable full structural dynamics to be reproduced, but the time required prohibits any prospect for use in an overall design tool. Recently, a combined approach using finite element method for the projectile and analytical functions for the target has been proposed for the simulation of penetration of aluminium, limestone or concrete target by spherical and ogive-nosed steel projectiles as discussed in [4] and in Refs. [10-14]. In addition to the cost-efficiency of this combined approach, this method eliminates the need for a contact algorithm between target and projectile, and avoids the problem due to excessive mesh distorsion for the target in Lagrangian formulation. The finite element used in these computation was a classical three-dimensional hexahedral continuum elements for the projectile modelling. In this paper, a two-dimensional quasi axisymmetric element is fitted to impact problems in order to enhance even more the cost efficiency of the combined analytical and computational approach.

The finite element proposed in this work is an advanced version of the quasi-axisymmetric element COMU developed by the French Research Institute for Nuclear Energy (Commissariat à l'Energie Atomique) to predict buckling of thin shell structures for design. Buckling process in thin shell structures is particularly sensitive to the imperfections of the shells. In the COMU element formulation, the imperfections and displacements of the

shell structure are described by Fourier series on circumferences of the quasi-axisymmetric structure following an approach proposed by Wunderlich *et al.* ([15]). The behaviour of the structure submitted to static or dynamic loads is computed from a finite element analysis by selecting a series of Fourier modes, on which are decomposed all physical values such as displacements, velocities, accelerations and forces. Strains and stresses are expanded in Fourier series as well. Thanks to the modal description of physical values on circumferences of the structure, imperfections and non axisymmetric loads are taken into account. So, the formulation enables to deal with three-dimensional problems, such as projectile impacting complex targets, while keeping the advantage of the two-dimensional analysis with low computation costs. To summarize, the COMU element has the following main features: non axisymmetric imperfection, non axisymmetric load, large displacements, non linear behaviour, low computation costs.

The initial formulation of this element has been improved in order to reproduce large rotations, that projectile may experience during the penetration into the target. To this end, the initial formulation based on an updated Lagrangian formulation is changed into a total Lagrangian formulation. In the following, the general formulation of the advanced COMU element will be presented in detail by pointing out the differences between the previous formulation and the new one. The COMU element developed in a total Lagrangian formulation is employed to reproduce penetration experiments reported by Frew *et al.* [3] involving limestone targets and ogive-nosed VAR 4340 steel projectiles. The target model is based on Forrestal's semi-empirical closed-form expression for the final depth of penetration. Values of limestone target resistance obtained by fitting the depth of penetration versus striking velocity data curve, are given by the authors. For the reproduction of the loss of confinement due to the entrance cratering effects, the methodology of successive layers proposed by Warren [4] is adopted. Results from non linear dynamic analyses with advanced COMU elements in terms of depth of penetration and projectile deformation through penetration are compared with experimental data and numerical results obtained by Warren using a three-dimensional finite element for the projectile.

2. GENERAL FORMULATION OF STRAINS FOR A SHELL

2.1 General formulation of strains for a geometrically perfect shell

In this first section, a geometrically perfect shell is considered. In other words, the initial imperfections of the shell structure are neglected.

Let us introduce a cylindrical coordinate system $(\vec{e}_r, \vec{e}_\theta, \vec{e}_z)$ where each point has three coordinates (r, θ, z), referring to the radius, the circumferential angle and the vertical coordinate, respectively. At a point M, the local reference is denoted by $(\vec{n}, \vec{s}, \vec{t})$, where $\vec{n}$ is the inward normal of the shell, $\vec{s}$ is the tangent vector along the meridian direction and $\vec{t}$ is the tangent vector along the circumference of the structure. We consider a conical shell, that is the curvature radius in the meridian plane $(\vec{n}, \vec{s})$, is assumed as infinite. In the meridian plane, the orientation of the conical shell is given by the angle $\varphi = (-\vec{e}_z, \vec{s})$.

The displacement field in the local coordinates is :

$$q = {}^t\{u \quad w \quad v \quad \beta\} \tag{1}$$

where u is the axial tangential displacement, w is the normal displacement to the shell, v is the circumferential tangential displacement, and β is the rotation of the shell around the tangential vector $\vec{t}$.

In the cylindrical system $(\vec{e}_r, \vec{e}_z, \vec{e}_\theta)$, the displacement field is denoted by :

$$\overline{q} = {}^t\{\overline{u} \quad \overline{w} \quad \overline{v} \quad \overline{\beta}\} \tag{2}$$

with
$$\begin{cases} w = \overline{u}\cos\varphi + \overline{w}\sin\varphi \\ u = \overline{u}\sin\varphi - \overline{w}\cos\varphi \\ v = \overline{v} \\ \beta = \overline{\beta} \end{cases} \tag{3}$$

The rotations of the shell around the tangent vector $\vec{s}$ and normal vector $\vec{n}$ are not taken into account.

The strain tensor is given by :

$$\varepsilon(q) = \frac{1}{2}\left(\nabla q + {}^t\nabla q\right) + \frac{1}{2}\left({}^t\nabla q . \nabla q\right) \tag{4}$$

where the gradient operator is expressed on the perfect configuration.

The tensor can be decomposed into two parts, as follows :

$$\varepsilon(q) = \varepsilon^L(q) + \varepsilon^Q(q) \tag{5}$$

where $\varepsilon^L(q)$ is the linear part of strains, and $\varepsilon^Q(q)$ is the quadratic part of strains involved in buckling and large displacement analysis.

Let us write the linear strains in the following vector form :

$$\varepsilon^{L}(q)=\begin{bmatrix}\varepsilon_{ss}^{Lm}\\ \varepsilon_{\theta\theta}^{Lm}\\ 2\varepsilon_{s\theta}^{Lm}\\ \chi_{ss}^{L}\\ \chi_{\theta\theta}^{L}\\ 2\chi_{s\theta}^{L}\end{bmatrix}=\begin{bmatrix}\{\varepsilon^{Lm}\}\\ \{\chi^{L}\}\end{bmatrix} \tag{6}$$

$\{\varepsilon^{Lm}\}$ being the linear membrane strains and $\{\chi^{L}\}$ the linear changes of curvature.

For a flat shell with a infinite curvature radius in the meridian plane, the expressions of linear membrane deformations are :

$$\begin{aligned}\varepsilon_{ss}^{Lm}&=\left(\frac{\partial u}{\partial s}\right)\\ \varepsilon_{\theta\theta}^{Lm}&=\left(\frac{1}{r}\frac{\partial v}{\partial\theta}+\frac{w}{r}\cos\varphi+\frac{u}{r}\sin\varphi\right)\\ \varepsilon_{s\theta}^{Lm}&=\frac{1}{2}\left(\frac{1}{r}\frac{\partial u}{\partial\theta}-\frac{v}{r}\sin\varphi+\frac{\partial v}{\partial s}\right)\end{aligned} \tag{7}$$

and the linear changes of curvature variations are given by :

$$\begin{aligned}\chi_{ss}^{L}&=\left(-\frac{\partial^2 w}{\partial s^2}\right)\\ \chi_{\theta\theta}^{L}&=\frac{1}{r^2}\left(-\frac{\partial^2 w}{\partial\theta^2}-r\sin\varphi\frac{\partial w}{\partial s}+\cos\varphi\frac{\partial v}{\partial\theta}\right)\\ \chi_{s\theta}^{L}&=\frac{1}{2r^2}\left(-2r\frac{\partial^2 w}{\partial\theta\partial s}+r\cos\varphi\frac{\partial v}{\partial s}-v\cos\varphi\sin\varphi+\frac{\partial w}{\partial\theta}\sin\varphi\right)\end{aligned} \tag{8}$$

The shear strain in the thickness of the shell is expressed as :

$$\varepsilon_{\xi s}^{L}=\frac{1}{2}\left[\frac{\partial w}{\partial s}+\beta\right] \tag{9}$$

The Kirchoff-Love relation, classically assumed for thin shells, states that linear shear strain $\varepsilon_{\xi s}$ can be neglected. Consequently, the component β of the displacement field is linked to the longitudinal derivative of the normal displacement. We have :

$$\beta=-\frac{\partial w}{\partial s} \tag{10}$$

Thus, the first curvature term in (8) becomes :

$$\chi_{ss}=\frac{\partial\beta}{\partial s} \tag{11}$$

For the quadratic part of the strain tensor, only membrane strains are taken into account, as classically assumed for thin shells. The non linear membrane strains are given by :

$$\begin{aligned}
\varepsilon_{ss}^{Qm} &= \frac{1}{2}\left[\left(\frac{\partial w}{\partial s}\right)^2+\left(\frac{\partial u}{\partial s}\right)^2+\left(\frac{\partial v}{\partial s}\right)^2\right] \\
\varepsilon_{\theta\theta}^{Qm} &= \frac{1}{2r^2}\left[\left(\frac{1}{r}\frac{\partial w}{\partial \theta}-v\cos\varphi\right)^2+\left(\frac{\partial u}{\partial \theta}-v\sin\varphi\right)^2+\left(\frac{\partial v}{\partial \theta}+w\cos\varphi+u\sin\varphi\right)^2\right] \\
\varepsilon_{s\theta}^{Qm} &= \frac{1}{2r}\left[\left(\frac{\partial w}{\partial \theta}-v\cos\varphi\right)\left(\frac{\partial w}{\partial s}\right)+\left(\frac{\partial u}{\partial s}\right)\left(\frac{\partial u}{\partial \theta}-v\sin\varphi\right)+\frac{\partial v}{\partial s}\left(\frac{\partial v}{\partial \theta}+w\cos\varphi+u\sin\varphi\right)\right]
\end{aligned} \tag{12}$$

At a point M located in the thickness of the shell from a distance ξ to the neutral fibre, the total strain is given by :

$$\left\{\varepsilon^T\right\}=\begin{bmatrix}\varepsilon_{ss}^T\\ \varepsilon_{\theta\theta}^T\\ 2\varepsilon_{s\theta}^T\end{bmatrix}=\left\{\varepsilon^{Lm}\right\}+\xi\left\{\chi^L\right\}+\left\{\varepsilon^{Qm}\right\} \tag{13}$$

with

$$\varepsilon^Q(q)=\left\{\varepsilon^{Qm}\right\}=\begin{bmatrix}\varepsilon_{ss}^{Qm}\\ \varepsilon_{\theta\theta}^{Qm}\\ 2\varepsilon_{s\theta}^{Qm}\end{bmatrix} \tag{14}$$

2.2 General formulation of strains for a geometrically imperfect shell

The previous section provided analytical expressions for linear and non linear strains as a function of the displacement field q from a perfect axisymmetric structure. Let us now introduce an initial imperfection field. The imperfect shell with geometrical imperfections, denoted by I, is related to a virtual perfect shell, denoted by P, through a displacement field, denoted by D. When a load F is applied to the actual structure, the structure experiences a displacement field, denoted by q.

The purpose is to express the strain tensor induced by the imperfection field D and the incremental displacement q on the perfect configuration P. The methodology, which has been first proposed by Marguerre for a general tridimensional problem, is applied here to the case of an axisymmetric structure with non-axisymmetric imperfections of any size. On the imperfect configuration I, the strain tensor induced by the incremental displacement follows the previous expression (4).

The strain tensor associated with the displacement field q can be obtained on the perfect configuration P by introducing the initial displacement field D :

$$\varepsilon(D,q)=\varepsilon(D+q)-\varepsilon(D) \tag{15}$$

After expanding the terms of the above expression, we obtain the following expression for the strain tensor expressed on the perfect configuration :

$$\varepsilon^{NL}(D,q)=\varepsilon^L(q)+\varepsilon^Q(q,D)+\varepsilon^Q(D,q)+\varepsilon^Q(q,q) \tag{16}$$

where quadratic terms of the strain tensor are defined by the quadratic operator :

$$\varepsilon^{Q}(q_1, q_2) = \frac{1}{2}\left[{}^{t}\nabla q_1 . \nabla q_2\right] \tag{17}$$

the gradient operator of the displacement fields q_1 and q_2 being defined on the perfect configuration P.

It is worth noting that, at this point, no assumption on the size of initial imperfections and displacements is made. The original version of the quasi-axymmetric COMU element assumes that the incremental displacement q is small with respect to the initial imperfection D, so that the quadratic term of displacement $\varepsilon^{Q}(q,q)$ could be neglected.

When considering an initial perfect axisymmetric structure, the linear and non linear strains coming from the displacements of the shell are given in Equations (7) to (12) in local coordinates. In a classical finite element formulation, these strains can be linked to the displacements of the nodes of the shell element through divergence operators. After expanding the imperfection displacements in Fourier series, it will be shown in the following that the divergence operators for strains can be also expanded in Fourier series.

Expressions of the linear strains $\varepsilon^{L}(q)$ and non linear strains $\varepsilon^{Q}(q,q)$ for the perfect shell will be further employed to derive the total strains $\varepsilon^{NL}(D,q)$ for an imperfect shell. The general outline of the formulation is to express strain and stress Fourier coefficients for a given COMU element as a function of Fourier coefficients of the nodal displacements in cylindrical coordinates.

3. FOURIER DECOMPOSITION OF STRAINS AND STRESSES FOR A GEOMETRICALLY IMPERFECT SHELL

3.1 Decomposition of the displacement field into Fourier series

By referring to the perfect configuration in local coordinates, the displacement field can be expanded in a Fourier series:

$$q = q_0 + \sum_{n=1}^{N}\left[q^{S}(n) + q^{A}(n)\right] \tag{18}$$

where q_0 is a vector composed of four Fourier coefficients on the axisymmetric mode, $q^S(n)$ is associated with the n symmetric harmonic (symmetric with respect to the circumferential angle $\theta = 0$), and, $q^A(n)$ is associated with the n antisymmetric harmonic (symmetric with respect to the circumferential angle $\theta = \frac{\pi}{2}$).

So, in local coordinates, the four modal displacement vectors are :

$$q(n=0) = \begin{bmatrix} u(n=0) \\ w(n=0) \\ v(n=0) \\ \beta(n=0) \end{bmatrix}, \quad q^S(n) = \begin{bmatrix} u^S(n)\cos n\theta \\ w^S(n)\cos n\theta \\ v^S(n)\sin n\theta \\ \beta^S(n)\cos n\theta \end{bmatrix}, \quad q^A(n) = \begin{bmatrix} u^A(n)\sin n\theta \\ w^A(n)\sin n\theta \\ v^A(n)\cos n\theta \\ \beta^A(n)\sin n\theta \end{bmatrix} \tag{19}$$

In the following, for the sake of clarity, only symmetric harmonics will be considered. Formula for antisymmetric harmonics are deduced from those for symmetric harmonics by swapping $\cos n\theta$ factors with $\sin n\theta$ factors.

3.2 Geometry of the finite element and vector notations

The COMU element is a flat shell element, with two nodes i and j. The geometry of the shell element is defined by the longitudinal length L, the radius at the middle of the element R_m, the thickness e, and the orientation angle $\varphi = (-\vec{e}_z, \vec{s})$. The shape functions are linear. In local coordinates, we have :

$$f = \frac{1}{2}(1-x)\, f_i + \frac{1}{2}(1+x)\, f_j \tag{20}$$

where f_i and f_j refer to one of degrees of freedom, that is the displacements (u, w, v) or the rotation (β), at nodes i and j in local coordinates, respectively ; x is the finite element parametric variable along the longitudinal local direction $\vec{s}$, equal to -1 at node i, 0 at the middle the element and +1 at node j.

The partial derivative along the longitudinal direction is given by :

$$\frac{\partial f}{\partial s} = \frac{2}{L}\frac{\partial f}{\partial x} \tag{21}$$

where f can be replaced with the displacements (u, w, v) or the rotation (β).

The displacement field in local coordinates can be expressed in cylindrical coordinates according to (3).

In the cylindrical reference, let us write the displacement vector for the shell element on the n symmetric harmonic ; this one is composed of two parts associated with the two nodes i and j of the element under consideration :

$$\left\{\overline{q}^{S}(n)\right\}=\begin{bmatrix}\left\{\overline{q}_i^{S}(n)\right\}\\ \left\{\overline{q}_j^{S}(n)\right\}\end{bmatrix} \tag{22}$$

where displacement vectors of nodes i and j on the n symmetric harmonic are written as :

$$\begin{aligned}{}^{t}\left\{\overline{q}_i^{S}(n)\right\}&=\left[\overline{u}_i^{S}(n)\quad \overline{w}_i^{S}(n)\quad \overline{v}_i^{S}(n)\quad \overline{\beta}_i^{S}(n)\right]\\ {}^{t}\left\{\overline{q}_j^{S}(n)\right\}&=\left[\overline{u}_j^{S}(n)\quad \overline{w}_j^{S}(n)\quad \overline{v}_j^{S}(n)\quad \overline{\beta}_j^{S}(n)\right]\end{aligned} \tag{23}$$

The axisymmetric $\left\{\overline{q}\ (n=0)\right\}$ follow an analogous expression.

Note that these vectors are composed of Fourier coefficients. In the cylindrical reference, the total displacement of the node i is obtained by recomposing the Fourier series :

$$\begin{cases}\overline{u}_i=\overline{u}_i(n=0)+\sum_{n=1}^{N}\overline{u}_i^{S}(n)\cos n\theta\\ \overline{w}_i=\overline{w}_i(n=0)+\sum_{n=1}^{N}\overline{w}_i^{S}(n)\cos n\theta\\ \overline{v}_i=\overline{v}_i(n=0)+\sum_{n=1}^{N}\overline{v}_i^{S}(n)\sin n\theta\\ \overline{\beta}_i=\overline{\beta}_i(n=0)+\sum_{n=1}^{N}\overline{\beta}_i^{S}(n)\cos n\theta\end{cases} \tag{24}$$

In the following, we will express the linear and non linear strains in the (i,j) element as a function of the modal displacements $\left\{\overline{q}\ (n=0)\right\}$ and $\left\{\overline{q}^{S}(n)\right\}$ in the cylindrical reference, by considering an element without geometric imperfection. The case of the geometrically imperfect element with an initial imperfection field D will be later deduced from these expressions.

3.3 Fourier decomposition of linear strains for a geometrically perfect element

We seek to express the linear strains $\varepsilon^{L}(q)$, in terms of modal displacement vectors $\left\{\overline{q}\ (n=0)\right\}$ and $\left\{\overline{q}^{S}(n)\right\}$ in cylindrical coordinates.

Firstly, let us consider the local displacements on the axisymmetric mode : $u=u(n=0)$, $w=w(n=0)$, $v=v(n=0)$, $\beta=\beta(n=0)$. The expressions of linear strains, given in Equations (7) to (11), are developed by using the shape functions of the element (20), the relations between cylindrical coordinates and local coordinates (3), and the relation on the longitudinal derivative (21), in order to express linear strains as a function of the axisymmetric displacement $\left\{\overline{q}\ (n=0)\right\}$ in cylindrical coordinates. Finally, the linear strains associated with the axisymmetric mode of displacement can be written as :

$$\left\{\varepsilon^{L}(q)\right\}={}^{t}\left[\varepsilon_{ss}^{Lm}\quad \varepsilon_{\theta\theta}^{Lm}\quad 2\varepsilon_{s\theta}^{Lm}\quad \chi_{ss}^{L}\quad \chi_{\theta\theta}^{L}\quad 2\chi_{s\theta}^{L}\right]=\left[B_0\right]\left\{\overline{q}(n=0)\right\} \tag{25}$$

where the 6-by-8 matrix $[B_0]$ corresponds to the divergence operator associated with the axisymmetric mode. The same methodology is applied to the local displacements on the n symmetric. The n symmetric local displacement is defined by : $u = u(n)\cos n\theta$, $w = w(n)\cos n\theta$, $v = v(n)\sin n\theta$, $\beta = \beta(n)\cos n\theta$, θ being the circumferential angle. By introducing two 6-by-8 matrices $[B_c^S(n)]$ and $[B_s^S(n)]$ associated with a cosine factor and a sine factor, respectively, we can express the linear strains in the element in terms of the n symmetric displacement :

$$\{\varepsilon^L(q)\} = [B_c^S(n)]\{\overline{q}^S(n)\}\cos n\theta + [B_s^S(n)]\{\overline{q}^S(n)\}\sin n\theta \tag{26}$$

All the matrices $[B]$ introduced in the above expressions can be found in [2].

By adding the contributions of all the harmonics of the displacement and grouping the cosine and sine terms, the complete expression of the linear strains in the (i,j) element is expressed as :

$$\{\varepsilon^L(q)\} = \{\mathrm{B}(q)\} = \begin{bmatrix}\{\varepsilon^{Lm}\}\\ \{\chi^L\}\end{bmatrix} = [B_0]\{\overline{q}(n=0)\} + \sum_{n=1}^{N}\left([B_c^S(n)]\{\overline{q}^S(n)\}\right)\cos n\theta + \left([B_s^S(n)]\{\overline{q}^S(n)\}\right)\sin n\theta \tag{27}$$

3.4 Fourier decomposition of non linear strains for a geometrically perfect element

As previously carried out for the linear strains, the purpose is to link the non linear strains $\varepsilon^Q(q)$ to the modal displacement vectors of the two-nodes element.

Let us rewrite the non linear strain vector, given in (12), in the following product form :

$$\{\varepsilon^Q(q,q)\} = \begin{bmatrix}\varepsilon_{ss}^{Qm}\\ \varepsilon_{\theta\theta}^{Qm}\\ 2\,\varepsilon_{s\theta}^{Qm}\end{bmatrix} = \frac{1}{2}[H(q)]\{\Theta(q)\} \tag{28}$$

where the 6 components vector and 3-by-6 components matrix are given by :

$$\{\Theta(q)\} = \begin{bmatrix}\dfrac{\partial w}{\partial s}\\ \dfrac{\partial u}{\partial s}\\ \dfrac{\partial v}{\partial s}\\ \dfrac{1}{r}\left(\dfrac{\partial w}{\partial \theta} - v\cos\varphi\right)\\ \dfrac{1}{r}\left(\dfrac{\partial u}{\partial \theta} - v\sin\varphi\right)\\ \dfrac{1}{r}\dfrac{\partial v}{\partial \theta} + w\cos\varphi + u\sin\varphi\end{bmatrix} = \begin{bmatrix}\{\Theta_1(q)\}\\ \{\Theta_2(q)\}\end{bmatrix} \text{ and } [\mathrm{H}(q)] = \begin{bmatrix}{}^t\{\Theta_1(q)\} & [0\ \ 0\ \ 0]\\ [0\ \ 0\ \ 0] & {}^t\{\Theta_2(q)\}\\ {}^t\{\Theta_2(q)\} & {}^t\{\Theta_1(q)\}\end{bmatrix} \tag{29}$$

In order to derive the Fourier series of the non linear strains, we consider successively each modal displacements, following an analogous methodology as previously described.

Let us consider the axisymmetric local displacement. Using the relations (20), (3) and (21) (shape functions, transfer matrix and relation on the longitudinal derivative, respectively), the vector $\{\Theta(q)\}$ can be written as a product of a new 6-by-8 matrix $[G_0]$ and the axisymmetric displacement, as follows :

$$\{\Theta(q)\} = \left[{}^t\{\Theta_1(q)\} \quad {}^t\{\Theta_2(q)\} \right] = [G_0]\,\{\overline{q}(n=0)\} \tag{30}$$

From the above relation, the expression of the matrix $[\mathrm{H}(q)]$ on the axisymmetric mode is easily derived and is written as :

$$[\mathrm{H}(q)] = [A_0] \tag{31}$$

If we consider the n symmetric mode, matrices $[G_c^S(n)]$, $[G_s^S(n)]$ relate the vector $\{\Theta(q)\}$ to the modal displacements :

$$\{\Theta(q)\} = [G_c^S(n)]\{\overline{q}^S(n)\}\cos n\theta + [G_s^S(n)]\{\overline{q}^S(n)\}\sin n\theta \tag{32}$$

From the above expressions, $[\mathrm{H}(q)]$ matrices for the n symmetric displacement is given by :

$$[\mathrm{H}(q)] = \left([A_c^S(n)]\cos n\theta + [A_s^S(n)]\sin n\theta \right) \tag{33}$$

Complete expressions of the matrices $[G]$ and $[A]$ can be found in the [2].

Finally, by taking into account all the harmonics of the local displacement in the (i,j) element, we derive the complete expression of the non linear strains :

$$\{\varepsilon^Q(q,q)\} = \frac{1}{2}\left[[A_0] + \sum_{n=1}^{N} \left([A_c^S(n)]\cos n\theta + [A_s^S(n)]\sin n\theta \right) \right] \left[[G_0]\{\overline{q}_0\} + \sum_{p=1}^{N} \left([G_c^S(p)]\cos p\theta + [G_s^S(p)]\sin p\theta \right) \{\overline{q}^S(p)\} \right] \tag{34}$$

Products of two sine or cosine functions appear in the above expression. As a result, the Fourier series of non linear strains is truncated at an order corresponding to twice the order N of displacements.

3.5 Fourier decomposition of linear and non linear strains for a geometrically imperfect shell

The formulation of strains associated with a geometrically perfect shell enables the strains in the case of a geometrically imperfect shell to be expressed by substituting into the non linear part of the strain the imperfection field D for the displacement q .

As with the displacement field q , let us expand the imperfection field D into a Fourier series:

$$D = D_0 + \sum_{n=1}^{N} \left[D^S(n) \right] \tag{35}$$

Note that, unlike the original formulation of the quasi axisymmetric COMU element, the imperfection field incorporates here the axisymmetric harmonic. As a consequence, when non linear analysis is performed, the geometry of the perfect structure, on which the formulation is based, is not updated any more at each time step according to the incremental displacement associated with the mode axisymmetric. In this new formulation, all the geometry changes are taken into account in the imperfection field. Thus, the integration strategy of dynamic equations proposed in this paper uses a total Lagrangian formulation instead of an original updated Lagrangian formulation.

After changing q with D in the Equation (28), the linear and non linear strains (given in (16)) become :

$$\begin{aligned} \{\varepsilon^L(q)\} &= \{\mathrm{B}(q)\} \\ \{\varepsilon^{NL}(D,q)\} &= \frac{1}{2}[\mathrm{H}(q)]\{\Theta(q)\} + \frac{1}{2}[\mathrm{H}(D)]\{\Theta(q)\} + \frac{1}{2}[\mathrm{H}(q)]\{\Theta(D)\} \end{aligned} \tag{36}$$

where $\{\mathrm{B}(q)\}$ corresponds to the Fourier series of the linear part of the strains, whose complete expression can be decomposed in Fourier series in terms of $[B]$ matrices, as expressed in (27).

From (28), it is easily shown that we have : $[\mathrm{H}(D)]\{\Theta(q)\} = [\mathrm{H}(q)]\{\Theta(D)\}$ (37)

So, we obtain the reduced expression of the non linear strains :

$$\{\varepsilon^{NL}(D,q)\} = \left[\mathrm{H}(D + \frac{1}{2}q) \right] \{\Theta(q)\} \tag{38}$$

$\{\Theta(q)\}$ is expressed in terms of products of matrices $[G]$ by the displacement q.

$\left[\mathrm{H}(D + \frac{1}{2}q) \right]$ is expressed in terms of matrices $[A]$, which can be obtained from (29) holding for a perfect shell, by replacing the field displacement q with the field $D + \frac{1}{2}q$, that is, the sum of the imperfection field with the half of the displacement field.

3.6 Total Lagangian formulation

The computation follows the classical explicit scheme in a total Lagrangian formulation. The imperfection field D is equal to the displacement from the initial configuration at the impact time to the actual configuration at the

beginning of the time step under consideration. At a time step of the explicit scheme, the incremental displacement is Δq.

The matrices $[B]$, and $[G]$ are expressed here on the perfect initial configuration and are computed only at the beginning of the non linear analysis. The operators $[A]$ depend on the field $D+\frac{1}{2}\Delta q$, that is the displacement at the beginning of the time step added to the half of the incremental displacement. So, operators $[A]$ must be computed at each time step of the explicit scheme.

At a given time step, the incremental displacement Δq is deduced from the results on the previous time step defined by q, velocity $\dot{q}$ and acceleration $\ddot{q}$. The incremental linear and non linear strains are derived from the incremental displacement as follows :

$$\begin{aligned}\{\Delta\varepsilon^{L}(\Delta q)\} &= \{\mathrm{B}(\Delta q)\}\\ \{\Delta\varepsilon^{NL}(D,\Delta q)\} &= \left[\mathrm{H}(D+\frac{1}{2}\Delta q)\right]\{\Theta(\Delta q)\}\end{aligned} \tag{39}$$

The vectors and matrices involved in the above formula have been developed on a modal Fourier basis in Equations (27) and (38), by introducing the matrices $[B]$, $[A]$ and $[G]$.

As discussed previously, it is important to note that the axisymmetric mode is incorporated into the imperfection field D. This point is different from the original version of the quasi axisymmetric element, in which only non axisymmetric displacements are considered as imperfections. The original version based on an updated Lagrangian method is replaced by a total Lagrangian method.

Moreover, it is worth noting that the strain term $\frac{1}{2}[\mathrm{H}(\Delta q)]\{\Theta(\Delta q)\}$ in the full expression of strains (39) is taken into account in this new formulation at contrast to the original version of COMU element, in which the incremental displacement Δq was assumed to be small with respect to the imperfection field D.

3.7 Linear elastic stress-strain law

In large displacement analysis, we assume in this study that the Hooke's law is the same if expressed on the imperfect configuration or on the perfect one.

Under a plane stress assumption, the stresses are easily obtained from the strains. At a point located in the thickness of the shell from a distance ξ to the neutral fibre, the linear stress vector, composed of membrane and bending components, is :

$$\left\{\sigma^L(q)\right\}^t = \left[\sigma_{ss}^{Lm} \quad \sigma_{\theta\theta}^{Lm} \quad \sigma_{s\theta}^{Lm} \quad \sigma_{ss}^{Lb} \quad \sigma_{\theta\theta}^{Lb} \quad \sigma_{s\theta}^{Lb}\right] = \begin{bmatrix} [H] & 0 \\ 0 & \xi[H] \end{bmatrix} \left\{\varepsilon^L(q)\right\} \tag{40}$$

where the $[H]$ is the law matrix for an homogeneous, isotropic material under the plane stress assumption, defined by :

$$[H] = \frac{E}{1-\nu^2} \begin{bmatrix} 1 & \nu & 0 \\ \nu & 1 & 0 \\ 0 & 0 & \dfrac{1-\nu}{2} \end{bmatrix} \tag{41}$$

E being the Young's Modulus and ν the Poisson's ratio.

The non linear stress contains only membrane components and is written as :

$$\left\{\sigma^{NL}(D,q)\right\}^t = \left[\sigma_{ss}^{Qm} \quad \sigma_{\theta\theta}^{Qm} \quad 2\sigma_{s\theta}^{Qm}\right] = [H]\left\{\varepsilon^{NL}(D,q)\right\} \tag{42}$$

4. ANALYTICAL MODEL AND NUMERICAL SIMULATION

The approach adopted in this work lied in coupling analytical expressions representing the target resistance with a finite element method using COMU elements in a classical explicit scheme. First, we summarize the target resistance model based on Forrestal's semi-empirical closed-form expression for the final depth of penetration. Then, the target resistance model is incorporated into an explicit scheme involving COMU elements. The coupling technique between analytical forcing functions representing the target and the two-dimensional COMU modelling for the projectile is presented. Finally, the constitutive model used for the projectile is briefly described.

4.1 Target resistance model

The target resistance functions are implemented into the CalPen3D code (Sibeaud *et al.* [16], Buzaud *et al.* [17]) designed to provide an accurate determination of the curvilinear trajectory of a weapon while travelling through a three-dimensional target composed of concrete, rock, soil and air blocks. It has been extensively validated against a large experimental database in terms of depth of penetration, trajectory and time-history deceleration**.** CalPen3D has been developed in Java language, hence, it can be run on any operating system without compilation, provided the installation of the Java Virtual Machine.

The algorithm of CalPen3D is essentially based on the computation and summation of forces generated at the centre of each elementary four nodes flat surfaces on the outer surface of the projectile. Normal stresses generated at the projectile-target interface are obtained by using the spherical cavity-expansion solution (Refs [6-9]).

At each time step, the position of the centre of each element is checked to determine if a target element has been penetrated. In this case, local forces are applied at this position to resist the penetration of the projectile. Those forces are approximated assuming the expansion of a spherical cavity solution with the corresponding local normal velocity V_n. This results in a polynomial relation between the normal stress σ_n and the normal velocity V_n at the centre of the element:

$$\sigma_n = R + \rho_0 V_n^2 \tag{43}$$

where ρ_0 is the target density and R is the target strength resistance.

For limestone targets, Frew *et al.* [3] deduced from impact experiments involving ogive-nosed rod projectiles the following relation between the target resistance and projectile diameter:

$$R = K + k\left(\frac{2a_0}{2a}\right) \tag{44}$$

in which K and k are constants obtained from data fits, $2a_0$ is the reference projectile diameter, and $2a$ is the projectile diameter under consideration**.** Three sets of experiments had been carried out with 7.1, 12.7 and 25.4 mm projectile diameters. The constant values found by the authors are: $K = 607\,MPa$, $k = 86\ MPa$ and $2a_0 = 25.4\,mm$. The density of limestone target is equal to 2130 kg/m^3.

In this work, the three sets of penetration experiments published by Frew *et al.* are reproduced using a combined analytical and finite element method with COMU elements. All the VAR 4340 Rc 45 steel projectiles have a total length-to-diameter ratio of 10 and 3.0 caliber-radius-head (CRH) node shapes. The shank diameters and masses for each of the three sets of experiments are 25.4 mm, 0.931 kg (reference projectile); 12.7 mm, 0.117 kg; and 7.1 mm, 0.020 kg. So the target resistance parameters given by the relation (44) are 693 MPa, 779 MPa and 914 MPa with 25.4 mm, 12.7 mm and 7.1 mm projectile diameters, respectively. With this method accounting for the target resistance, all the constitutive behaviour of the target along with any frictional resistance is lumped into the previous expression (43).

Post-test observations [3] have exhibited a conical cratering region that is approximately two diameters in depth. This cratering region is followed by a tunneling region that is approximately one projectile diameter. Therefore,

the first region needs a special treatment to take into account the less resistance due to the crater formation. We use the same methodology as proposed by Warren [4]. The two diameters in depth cratering region is subdivided into a suite of uniformly spaced layers with increasing strength. The normal stress acting on the projectile outer surface is given by :

$$\sigma_i = \psi_i \sigma_n \tag{45}$$

with σ_n is the unreduced normal stress obtained from (43), and $\psi_i = 0.1i$, i being the layer index.

In this region, normal stresses are only allowed to act on the nose of the projectile and not the shank. In the tunneling region where the target material is confined and cannot be ejected out, unreduced normal stresses are applied to the whole outer surface of the projectile.

4.2 Non linear dynamic analyses

The analytical and numerical combined method as employed by Warren [4] is adopted in this work in order to simulate ogive-nosed steel rod projectiles impacting limestone targets. An explicit dynamic scheme with COMU elements has been implemented in the CalPend3D code in order to couple finite element method for the projectile with the analytical forcing functions representing the target.

The equation of equilibrium governing the dynamic response of the shell structure modelled with COMU elements is :

$$M\ddot{U} = F_{ext} - F_{\text{int}} \tag{46}$$

where M is the mass matrix decomposed in Fourier series, $\ddot{U}$ contains the Fourier coefficients of the nodal accelerations,

F_{ext} and F_{int} contain the Fourier coefficients of the external and internal forces, which will be explained in the following.

Non linear computations are here carried out using an explicit dynamic scheme. This method allows to use a diagonal mass matrix M (Belytschko *et al*. [18]) , which components are associated with the Fourier harmonics taken into account in the computations.

All the vectors involved in the momentum conservation are decomposed into Fourier series. Thus, for a given i node, Fourier coefficients of the acceleration are organised as follows : axisymmetric mode (p=0), p symmetric mode followed by p antisymmetric mode, with $p = 1 \ldots N$, N being the chosen truncature order for the displacement expansion in Fourier series. So, each node of the modelled axisymmetric structure has $4 + 8 \times N$

degrees of freedom. Note that a complete Fourier base truncated at the order N is used in this formulation, that is, all the harmonics of an order less than N are taken into account into the Fourier series.

In this work, the complete description of the projectile is provided by the Fourier coefficients displacement and velocity, contained in the global vectors U and $\dot{U}$ involved in the equilibrium equation. For each COMU node, P points regularly distributed along the circumference associated with the COMU node are taken into account. The displacement and velocity at each point along the circumference are obtained by recomposing Fourier series. So the position and velocity of each point are computed at each time step with respect to the initial referential, associated with the initial configuration of the structure at the impact time. The coordinates and velocities of these points in the target referential are then easily obtained by using a transfer matrix from the initial referential (at impact) to the target referential. After determining the Fourier coefficients of forces F_{ext} and F_{int}, the Fourier coefficients of the acceleration contained in the global vector $\ddot{U}$ are easily obtained by resolving the equation of motion with the diagonal mass matrix M.

4.3 COMU element coupling with then target resistance model

The two-dimensional finite element mesh with quasi-axisymmetric COMU elements to model the ogive-nosed projectiles in all of the simulations is illustrated in Fig. 1. The projectile is modelled with 10 elements for the nose and 20 elements in the shank part. The mesh is defined from a two-dimensional profile of 30 COMU nodes, located at the neutral fibre of the rod projectile. The forcing function due to the target resistance through the penetration process acts on the outer surface of the projectile. As discussed previously, displacements and velocities at a set of points regularly distributed along the circumference are known by recomposing Fourier series. As theses points are located at the neutral fibre, a technique is set up to reconstruct at each time step of the explicit scheme the actual configuration of the projectile outer surface. This is explained in the following.

For each circumference, we can deduce the point at the axis from the set of P points along the circumference. For a given circumference corresponding to a COMU node, we denote this point located at the axis Q_A. From each point Q located along the circumference at the neutral fibre, we can obtain an associated point Q' located on the outer surface of the projectile from:

$$\vec{u}' = \vec{u} + \frac{\vec{u}}{\|\vec{u}\|}\frac{e}{2} \tag{47}$$

where $\vec{u}$ is the vector from the point at the axis Q_A to Q at the neutral fibre and $\vec{u}'$ is the vector from Q_A to Q' located at the outer surface, and e is equal to the thickness associated with the considered circumference. In the general case, this corresponds to the shell thickness. Here, the thickness corresponds to the shank radius of the projectile rod.

With this method, the actual configuration of the outer surface of the projectile can be constructed at each time step. Fig. 2 illustrates the reconstruction technique of the outer surface from a deformed configuration at a given time during the penetration process: this configuration selected for illustration has been obtained in the initial impact referential at 260 μs for a 12.7 mm diameter projectile with a striking velocity of 457 m/s. This simulation will be presented in the section devoted to the numerical results. As it can be seen, the outer surface is finally composed of quadrilateral elementary flat surfaces.

On a given elementary quadrilateral side defined by 4 points composing the outer flat surface, the force acting on this side is given by :

$$df = \psi \left[R + \rho_0 \left(\vec{V}_I . \vec{n} \right)^2 \right] da \tag{48}$$

where $\vec{V}_I$ is equal to the mean velocity of the 4 points at the neutral fibre deduced by recomposing Fourier series of velocity, $\vec{n}$ is the outward unit vector normal to the diagonals of the outer quadrilateral side, ψ accounts for the cratering region, and da is the surface of the quadrilateral side. This force is then distributed to the 4 points at the medium fiber. The forces are then computed for the whole outer surface and are expanded along each circumference in Fourier series. Finally, we obtain the applied load vector F_{ext} involved in the equation of motion (46) whose components are Fourier coefficients of the external force decomposed on the projectile circumferences.

4.4 Constitutive model for VAR 4340 steel projectile

The constitutive model adopted is a simplified Johnson-Cook type model (assuming the material elastic-plastic without temperature influence), with a yield criterion for plasticity defined by :

$$f(\sigma, p) = \overline{\sigma} - \left(\sigma_e + B\, p^n \right) \tag{49}$$

where $\overline{\sigma}$ is the Von Mises stress, σ_e is the initial value of the yield surface, p is the effective plastic strain, B and n are the coefficients of the plastic law.

The model parameters are chosen so as to fit in a best way the constitutive model used by Warren [4]. As the model adopted in this work is a simple elastic-plastic model, we chose to fit the parameters against the elastic-viscoplastic model used by Warren at a nominal strain rate of 0.001. Fig. 3 compares the constitutive model of Warren with the elastic plastic model. Model parameters obtained from curve fits are: $\sigma_e = 1.04\ GPa$, $B = 0.99\ GPa$, and $n = 0.08$. The density, Young's modulus, and Poisson's ratio of the VAR 4340 Rc=45 steel are taken to be $\rho_0 = 7830\ kg/m^3$, $E = 206\ GPa$ and $\nu = \frac{1}{3}$, respectively.

At a time step of the dynamic explicit scheme, the plasticity is obtained for the set of points along each circumference of the projectile. By using a very classical initial stress method, the increment of plastic stress is numerically obtained. The plastic stresses around the circumference are then expanded in Fourier series with an order equal to N_σ. It is important to underline that the order of the truncated stress Fourier series N_σ must be sufficiently high so as to correctly reproduce the new distribution of plastic stresses. Otherwise, important bias could be engendered in the modal description of the physical plastic stresses.

These new Fourier coefficients of stresses are then used to calculate the internal force F_{int}. Due to the modal formulation of the element, the integration strategy employed here is particularly effective. The nodal forces are computed by integrating analytically the stresses on the circumference. Integration along the meridional direction is numerical and uses one Gauss point at the middle of the COMU element. Integration procedure can be found in Refs. [1-2]. As discussed previously, the external force F_{ext} is computed at each time step as well. A stabilisation force is added to avoid spurious vibrations. Indeed, Hourglass control is required because COMU element uses one integration point and under-integrates the element resulting in a rank deficiency which manifests itself into spurious zero energy modes that must be constrained. The stabilisation procedure used in this work is based on the transverse shear energy, which acts as a penalty that enforces the Kirchoff-Love constraint, given in (10). Transverse shears are assumed to be small, and the material response to such deformation is assumed to be linear elastic. Details about this classic method can be found in Hughes *et al.* [19] and Zienkiewicz *et al.* [20] works. Finally, the Fourier coefficients of forces are incorporated into the equation of motion (46).

5. RESULTS

In the following, results from non linear dynamic analyses with two-dimensional COMU elements are compared with experimental data obtained by Frew *et al.* [3] and numerical results published by Warren [4] using the same target model and three-dimensional constant strain hexahedral continuum elements. The purpose is to validate the low-cost numerical approach using the two-dimensional modal element COMU proposed in this paper.

The three dimensional outer surface reconstructed from the two-dimensional COMU profile is illustrated in Fig. 4. The same mesh is used in all of the simulations for the 25.4-mm-Diameter, 12.7-mm-Diameter and 7.1-mm-Diameter projectiles.

Table 1 summarizes penetration experiments and numerical results. There was no angle of obliquity with these experiments, so pitch and yaw angles are incorporated into a single angle of inclination. All of the COMU simulations are carried out with a modal basis containing 5 Fourier harmonics to represent displacements, velocities and accelerations. Thus the modal basis contains the axisymmetric mode, mode 1 symmetric and antisymmetric, and mode 2 symmetric and antisymmetric. That corresponds to $N = 2$ in (18). Along each circumference, 20 points regularly spaced are taken into account for the plasticity control. As explained in section 4.4, stress Fourier series must be sufficiently high so as to correctly reproduce the distribution of plastic stresses along circumferences. So we take an order of stress Fourier series equal to 10 that is 21 harmonics. All the simulations were run on a Pentium 4 (2.8 Ghz) computer with Windows system and the release 1.4 of the Sun Java 2 Platform, Standard Edition (J2SE) environment. Computation times were between 500 and 1200 CPUs depending on striking velocity. The computations times are approximately an order lower than that is reported with hexahedral elements (Warren [4], Warren *et al.* [10]). This is essentially due to the use of a two-dimensional mesh, the analytical stress integration along circumferences, and the fact that only one element COMU is required in the thickness of the rod projectile. It is also important to note that computations times given here are related to the interpreted Java language which has not the performance of a compiled language like Fortran. Authors believe that a more rigorous benchmark would be more clearly in favour of COMU approach.

5.1 The 12.7-mm-Diameter projectiles

In Table 1, it can be seen that numerical results in terms of depth of penetration using COMU element are consistent with experimental data. The analytical functions representing the target resistance applied to the outer surface of the projectile through penetration are derived from depth of penetration versus striking velocity data.

Therefore results validate the combined approach coupling finite element method and analytical functions to represent the target resistance.

Results obtained with COMU elements are also compared with numerical results using constant strain hexahedral continuum elements obtained by Warren. It is observed that depths of penetration are in good agreement with a maximum relative difference of 6 %. The same simulations as selected by Warren are chosen to compare the projectile deformations through penetration process. In Fig. 5, images at three specific times are shown for an impact with a velocity of 459 m/s and 3.55° of angle of inclination. The projectile deformations predicted by COMU elements are in very good agreement with those from three dimensional simulations. It is shown that the tail bends noticeably to the right, then reverses to the left. When travelling through the tunneling region, the projectile seems to be straightened out until it comes to rest at approximately 550 μs.

With a higher velocity of 1134 m/s and a 2.15° angle of inclination, the travel of the projectile through the target is illustrated in Fig. 6. Projectile configurations at three specific times are compared with those from Warren's computations. The bending of the projectile trough penetration is significantly higher than the previous simulation. The final configuration, which is consistent with the final configuration obtained by Warren and the experimental configuration after extracting the projectile from the target (photograph published by *Frew et al.* [3]), shows that the projectile is straightened out in the tunneling region. As it is has been underlined by Warren, COMU computations confirmed that projectile experiences strong bending at intermediate states although the recovered projectiles didn't show high levels of deformation. Note that depth of penetration predicted by COMU approach is higher than the 3D element approach (0.645 m and 0.608 m, respectively), but the projectile configurations at 90 μs and 150 μs with both 2D modal and 3D approaches are consistent.

5.2 The 25.4-mm-Diameter projectiles

Results in terms of depths of penetration are summarized in Table 1. The discrepancy between the simulations using COMU elements or 3D elements is very low with a relative difference less of 1 %. Inclination angles are low in all of these simulations so the trajectories through the limestone target are nearly straight. As the bending is also very reduced, projectile deformations are not shown for these simulations.

5.2 The 7.1-mm-Diameter projectiles

In Table 1 it is shown that discrepancy in terms of depth of penetration between the COMU simulation and 3D element simulation is less than 8 %, obtained with the lowest striking velocity. Otherwise the discrepancy

remains of an order of 3 %. The simulation of a 7.1-mm-Diameter projectile striking the limestone target with a velocity of 787 m/s and 1.25° angle of inclination is illustrated in Fig. 7 at three specific times. The bending of the tail to the left and to the right is well reproduced by the proposed COMU approach. With a higher velocity equal to 1340 m/s and a 2.01° angle of inclination, the tails whips back and forth into the tunneling region as shown in Fig. 8. Nonetheless it is observed that the projectile final configuration is slightly more tilted with COMU elements than 3D elements.

A final representation of the projectile travel through the limestone target is presented in Fig. 9 for a striking velocity of 1365 m/s and a 2.56° angle of inclination. Projectile trajectory through the target is obtained by plotting in the same figure different configurations at 125 different times (step time of 5 μs). A zoom on the tunneling region permits to exhibit the strong whipping of the tail. As Warren's computations, COMU simulations underpredict to a less extent depths of penetration for impact velocities of 1340 m/s and 1365 m/s with high angles of inclination. The reason conjectured by the authors lies in the fact that current expansion algorithm applies a load on the shank whenever there is a component of velocity in the outward normal direction and does not account for moved materials in the tunneling region.

7. CONCLUSION

The purpose of this work is to set up an effective two-dimensional modal finite element approach for simulating the dynamic structural behaviour of the projectile during a three-dimensional interaction with an infrastructure target. To this end, a modified formulation of the quasi-axisymmetric element COMU, based on the expansion of all the physical quantities into Fourier series, is proposed. This new formulation of 2D modal element COMU developed according to a total Lagrangian formulation has been detailed.

As regards penetration problems, the explicit scheme using new COMU elements has been implemented into the CalPen3D code. This simulation software uses an analytical approach, based on a spherical cavity-expansion approximation. The time integration in accordance with an explicit scheme using modified COMU elements allows to couple the two approaches, that is the finite element method to represent the deformation of the projectile and analytical method to represent the target.

Two-dimensional modal analyses have been performed to simulate ogive-nosed rod projectiles impacting limestone targets. Comparisons between experimental data and numerical results obtained with hexahedral

continuum elements to represent the projectile and the same target modelling enable to check the accuracy of the two-dimensional modal approach. Moreover, thanks to the two-dimensional modelling and the efficiency of the stress integration decomposed in Fourier series, the two-dimensional modal approach proposed in this paper is able to reduce significantly the computation time in comparison to a classical three-dimensional analysis. On account of its cost-efficiency, the quasi axisymmetric modal approach may be well suited for parametric studies in order to provide useful insight into the effects of several variables such as impact angles, velocity, material and geometric characteristics of the projectile and target.

Although the formulation of the COMU elements has been established for thin shell structures, we showed that COMU elements still provide accurate predictions for penetration problems involving steel rod projectiles. However, a limitation of the approach lies in the modal description of localisation process like damage or cracking: if a local damage appears (generated, for example, by a contact with a reinforced steel) the Fourier description with a few harmonics fails to reproduce the damage pattern. Use of higher order harmonics is still possible, but at a computational cost that makes COMU less attractive.

ACKNOWLEDGEMENTS

This work, carried out by the applied research office EC2-MS (Etudes, Conseils et Calculs en Mécanique des Structures), was funded by contract from Centre d'Etudes de Gramat, Délégation Générale pour l'Armement.

REFERENCES

1. A. Combescure. Static and dynamic buckling of large thin shells : design procedure, computation tools, physical understanding of the mechanisms. Nuclear Engineering and Design, **92**, 339-354, 1985.
2. A. Combescure. Etude de la stabilité non linéaire géométrique et non linéaire matériau des coques minces. Application aux coques de révolution avec imperfections soumises à des chargements complexes. Habilitation à Diriger des Recherches, INSA Lyon, 1995.
3. D.J. Frew, M.J. Forrrestal, S.J. Hanchak. Penetration Experiments With Limestone Targets and Ogive-Nose Steel Projectiles. Journal of Applied Mechanics, Vol **67**, pp 841-845, 2000.
4. T.L. Warren. Simulations of the penetration of limestone targets by ogive-nose 4340 steel projectiles. International Journal of Impact Engineering, **27**, 475-496, 2002.
5. C.W. Young. Simplified Analytical Model of Penetration with Lateral Loading : user's guide. Sandia National Laboratories, Albuquerque, NM 87110, USA, 1998.
6. M.J. Forrestal, V.K. Luk. Penetration into soil targets. International Journal of Impact Engineering, **12**, 427-444, 1992.
7. M.J. Forrestal. Penetration into dry porous rock. International Journal of Solids and Structures, N°12, Vol 22, 1485-1500, 1986.
8. V.K. Luk, M.J. Forrestal. Penetration into semi-infinite reinforced-concrete targets with spherical and ogival nose projectiles. International Journal of Impact Engineering, **6**, 291-301, 1987.
9. M.J. Forrestal, D.J. Frew, J.P. Hickerson, T.A. Rohwer. Penetration of concrete targets with deceleration-time measurements. International Journal of Impact Engineering, **28**, 479-497, 2003.
10. T.L. Warren, S.J. Hanchak, K.L. Poormon. Penetration of limestone targets by ogive-nosed VAR 4340 steel projectiles at oblique angles: experiments and simulations. International Journal of Impact Engineering, **30**, 1307-1331, 2004.
11. T.L. Warren, K.L. Poormon. Simulations of the penetration of 6061-T6511 aluminium targets by spherical-nosed VAR 4340 steel projectiles. International Journal of Solids and Structures, 37, 4419-4435, 2000.
12. T.L. Warren, K.L. Poormon. Penetration of 6061-T6511 aluminium targets by ogive-nosed VAR 4340 steel projectiles at oblique angles. International Journal of Impact Engineering, **25**, 993-1022, 2001.
13. T.L. Warren, A.F. Fossum, D.J. Frew. Penetration into low-strength (23 MPa) concrete: target characterization and simulations. International Journal of Impact Engineering, **30**, 477-503, 2004.

14. K.T. Danielson, M.D. Adley. A meshless treatment of three-dimensional penetrator targets for parallel computation. Computational Mechanics, **25**, 267-273, 2000.

15. W. Wunderlich, H. Cramer and H. Obrecht, Application of ring elements in the non linear analysis of shells of revolution under non axisymmetric loading. Computer Methods in Applied Mechanics and Engineering, 51(3), 259-275 (1985).

16. J-M. Sibeaud, A. Delmas, T. Lacaze, CalPen3D: A three-dimensional penetration code suitable for Hardened Target Defeat Modeling – Numerical and Experimental assessment. 21 st International Symposium on Ballistics, Adelaide, Australia – 19-23 April 2004.

17. E. Buzaud, R. Laurensou, P. Belouet, C. Lissayou, An experimental investigation of corner effects resulting from vertical attack on hardened structures. 11 th International Symposium on Interaction of the Effects of Munitions with Structures, Mannheim, Germany – 05-09 May 2003.

18. T. Belytschko, W. Kam Liu, B. Moran, Nonlinear Finite Elements for Continua and Structures. Wiley (2000).

19. T.J.R. Hughes, R.L. Taylor and W. Kanoknukulchai. A simple and efficient finite element for plate bending. International Journal of Numerical Methods in Engineering, 11, pp 1529-1543, 1977.

20. O.C. Zienkiewicz, J. Bauer, K. Morgan and E. Onate. International Journal of Numerical Methods in Engineering, 11, pp 1545-1558, 1977.

List of legends

Figure 1. 2D modelling of the projectile with COMU elements

Figure 2. Reconstruction of the outer surface of the projectile from modal displacements in the target reference: (a) points at neutral fibre; (b) points at projectile axis; (c) points on the outer surface; (d) outer surface of the projectile

Figure 3. Comparison of constitutive models for VAR 4340 Rc=45 steel at nominal strain rate of $\dot{\varepsilon} = 0.001\ 1/s$

Figure 4. 3D geometry of the projectile reconstructed from the 2D COMU profile.

Figure 5. Simulation of a 12.7mm-Diameter projectile penetrating a limestone target at 459 m/s and 3.55° angle of inclination; left side Warren's results with 3D elements [4] and right side results with COMU elements

Figure 6. Simulation of a 12.7mm-Diameter projectile penetrating a limestone target at 1134 m/s and 2.15° angle of inclination; left side Warren's results with 3D elements [4] and right side results with COMU elements

Figure 7. Simulation of a 7.1 mm-Diameter projectile penetrating a limestone target at 787 m/s and 1.25° angle of inclination; left side Warren's results with 3D elements [4] and right side results with COMU elements

Figure 8. Simulation of a 7.1 mm-Diameter projectile penetrating a limestone target at 1340 m/s and 2.01° angle of inclination; left side Warren's results with 3D elements [4] and right side results with COMU elements

Figure 9. Penetration trajectory of a 7.1 mm-Diameter projectile penetrating a limestone target at 1365 m/s and 2.56° angle of inclination; zoom on the tail whipping back and forth

Table 1. Penetration results : depth of penetration P experimental data, numerical results with 3D element (Warren [4]) and with COMU elements; Relative difference between the numerical results.

Velocity (m/s)	Inclination (degree)	Experimental P	SCE/PRONTOD 3D P (m)	COMU 2D P	Relative difference
Diameter projectiles (12.7 mm)					
459	3.55	0.141	0.137	0.137	0 %
608	1.41	0.232	0.230	0.229	-0.5 %
853	0.00	0.362	0.418	0.417	-0.2 %
956	0.30	0.523	0.508	0.506	-0.4 %
1134	2.15	0.562	0.608	0.645	+6 %
1269	0.00	0.812	0.812	0.808	-0.5 %
1404	0.70	0.924	0.931	0.945	+1.5 %
1502	0.70	1.017	1.035	1.048	+1.2 %
Diameter projectiles (25.4 mm)					
407	0.64	0.260	0.261	0.261	0 %
566	0.60	0.390	0.454	0.452	-0.4 %
800	0.61	0.790	0.826	0.820	-0.7 %
917	0.30	1.020	1.045	1.036	-0.9 %
1177	0.30	1.500	1.579	1.563	-1 %
Diameter projectiles (7.1 mm)					
497	0.75	0.067	0.086	0.079	-8 %
597	0.50	0.105	0.110	0.107	-2.7 %
787	1.25	0.165	0.174	0.170	-2.3 %
795	0.50	0.178	0.180	0.176	-2.2 %
1037	0.90	0.271	0.280	0.274	-2.1 %
1060	0.56	0.294	0.295	0.287	-2.7 %
1230	0.25	0.392	0.379	0.368	-2.9 %
1340	2.01	0.437	0.389	0.400	+2.8 %
1365	2.56	0.430	0.369	0.383	+3.8 %
1516	1.42	0.516	0.516	0.500	-3.1 %

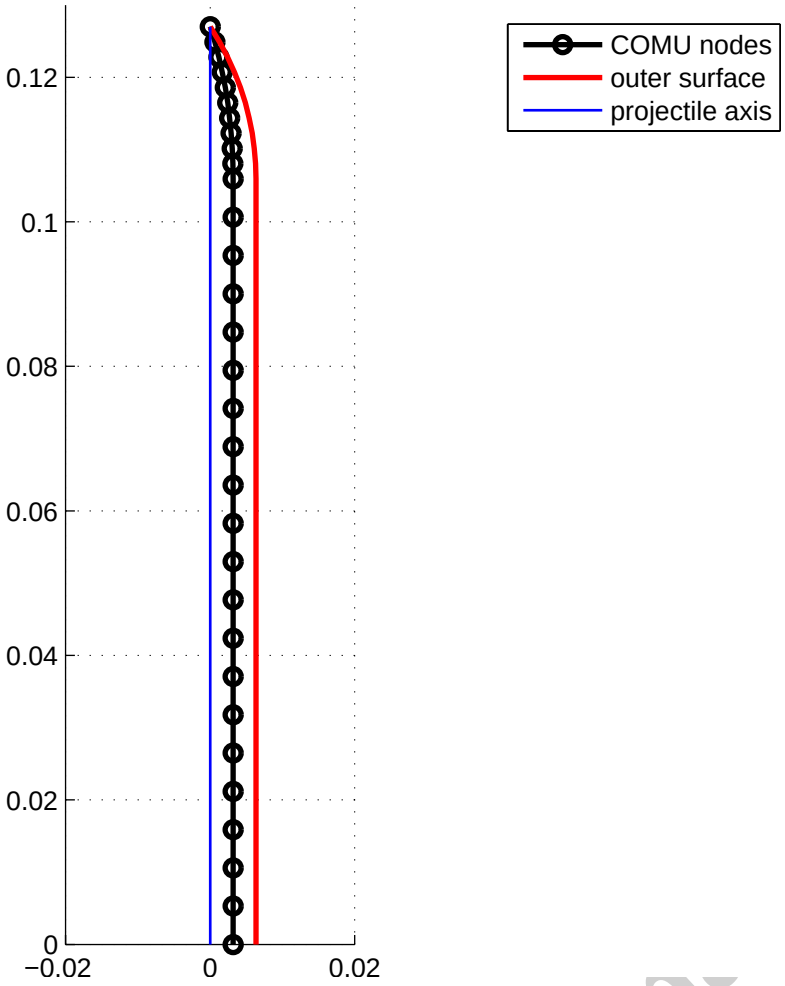

Figure 1.

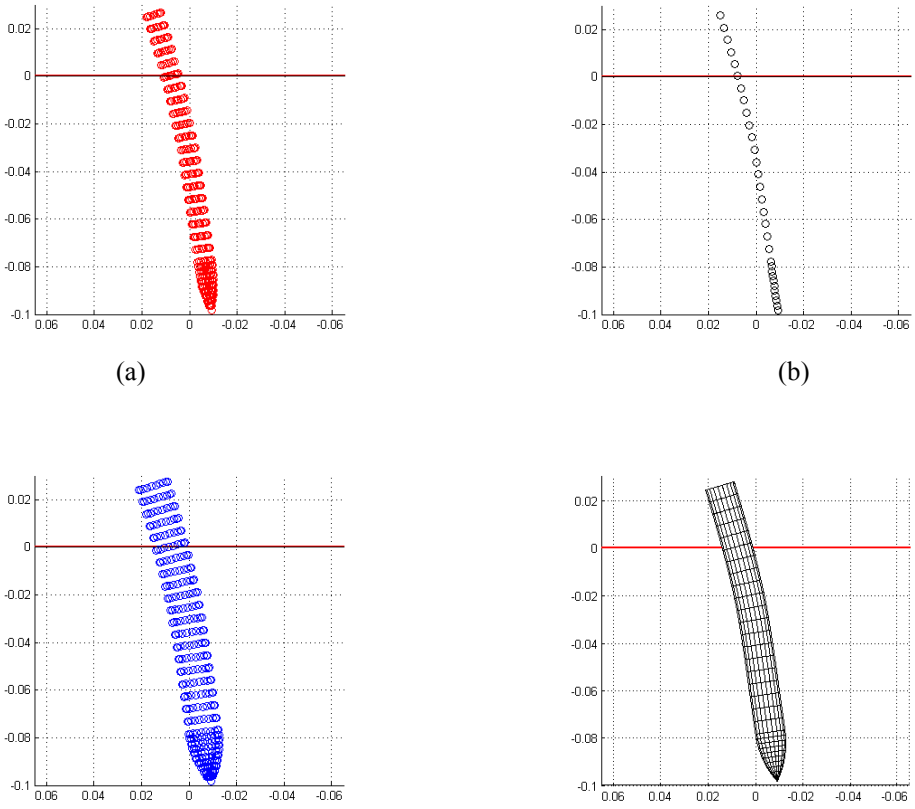

(a) (b)

(c) (d)

Figure 2.

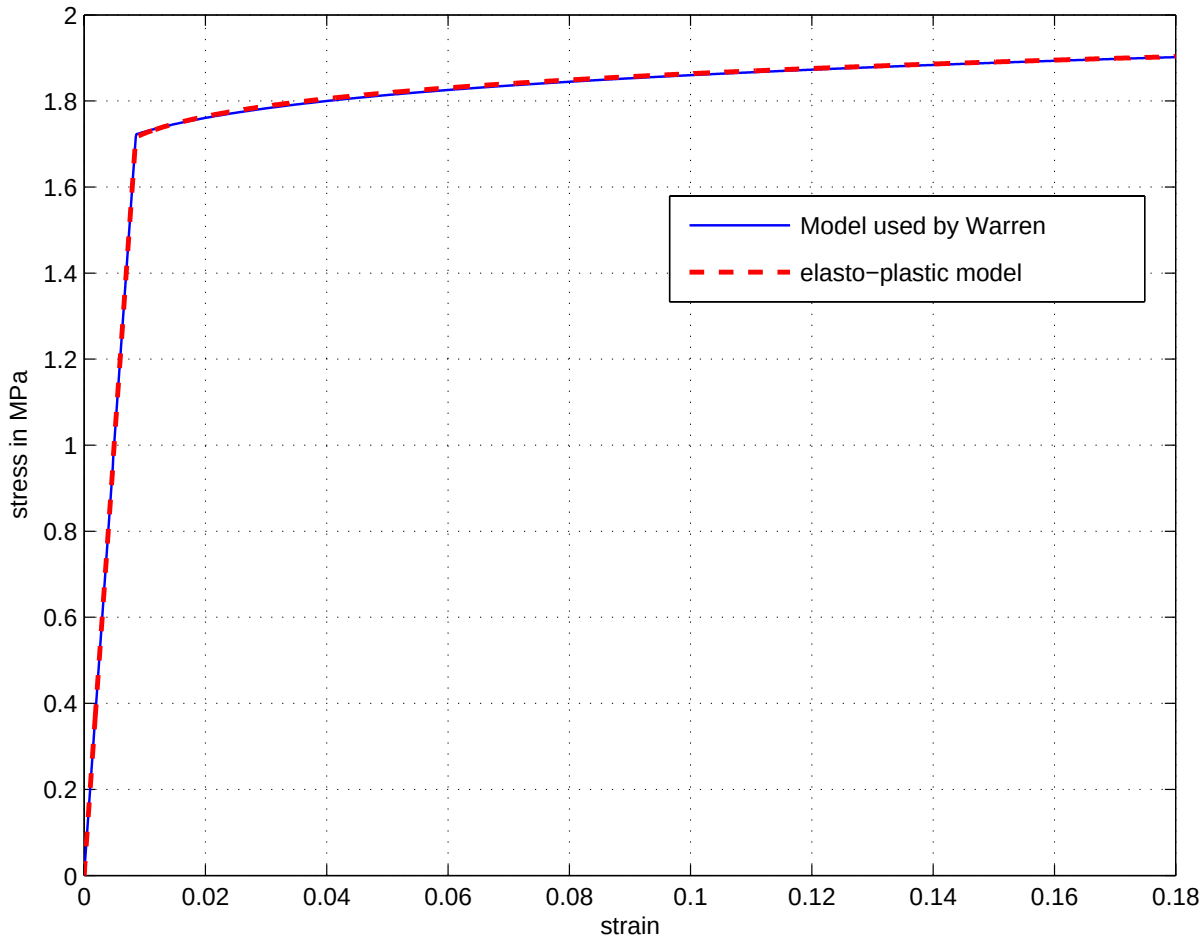

Figure 3.

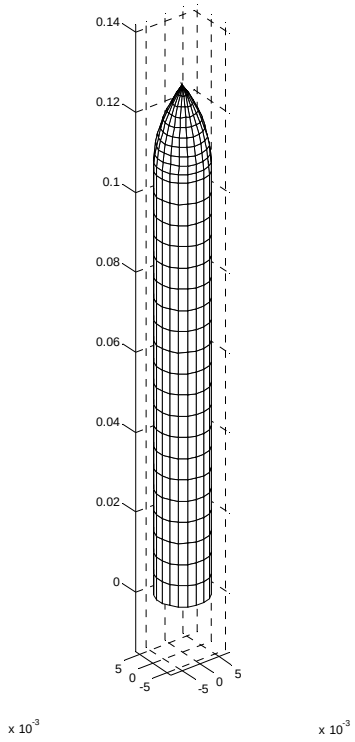

Figure 4.

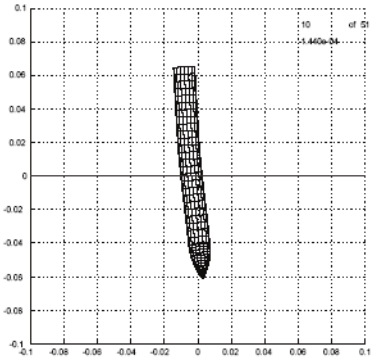

t = 144 μs

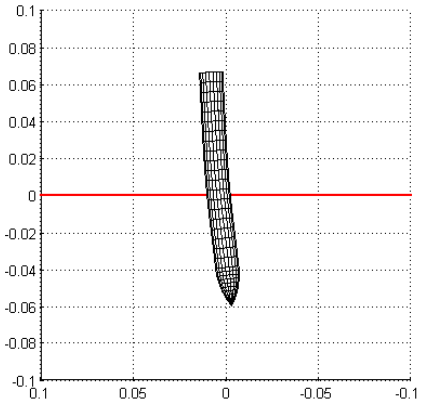

t = 140 μs

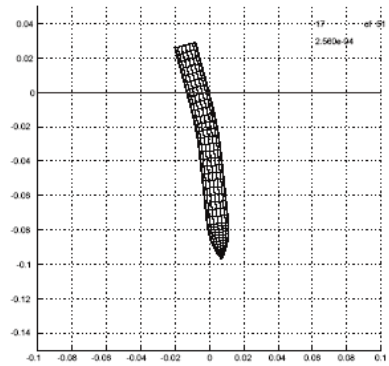

t = 256 μs

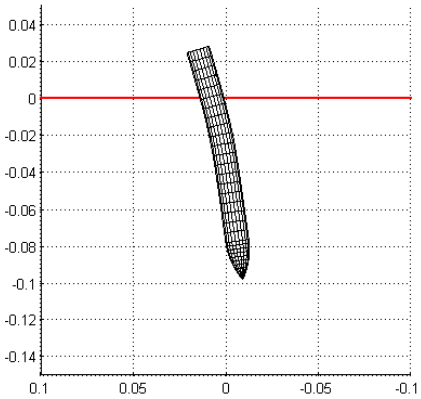

t = 260 μs

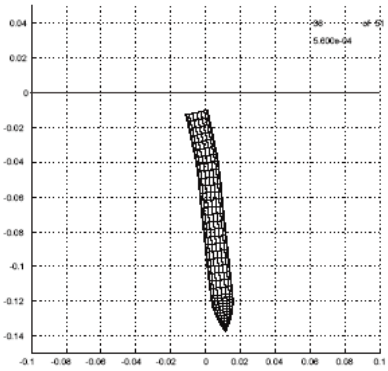

t = 560 μs

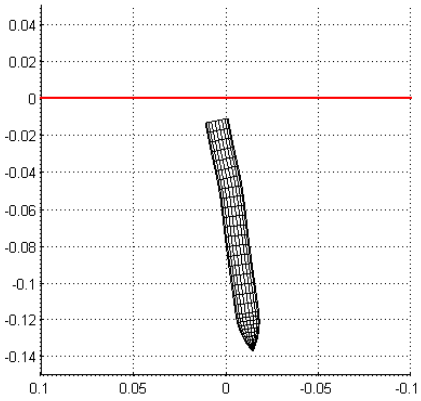

t = 550 μs

Figure 5.

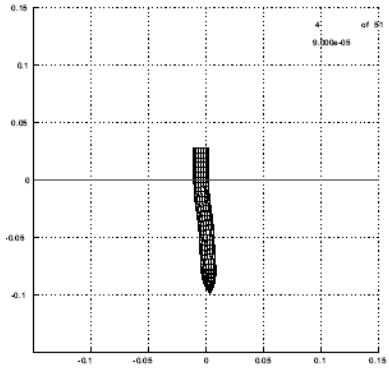

t = 90 μs

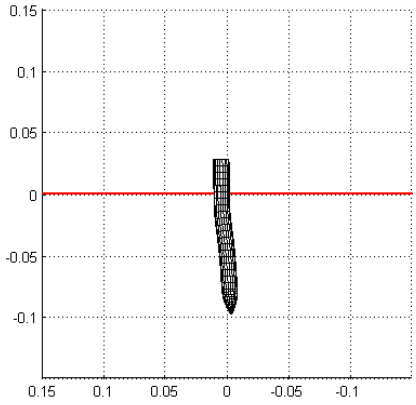

t = 90 μs

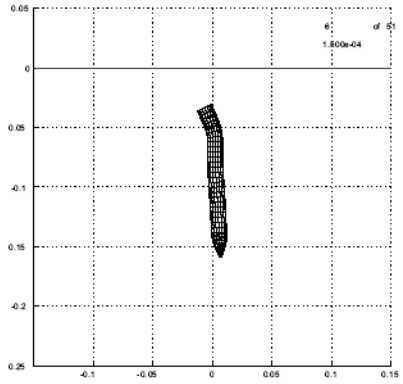

t = 150 μs

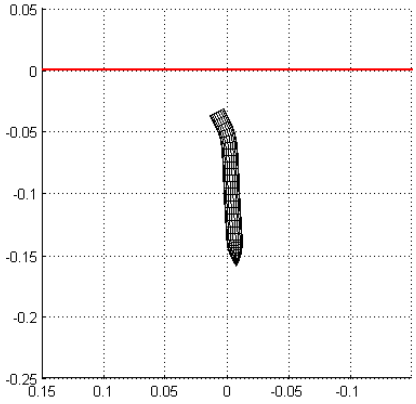

t = 150 μs

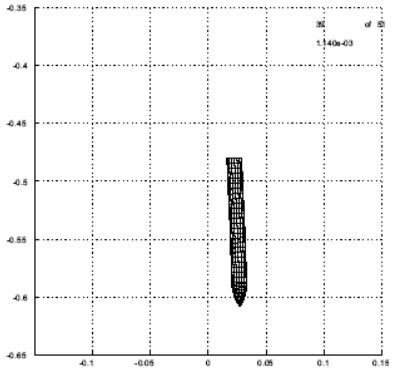

t = 1140 μs

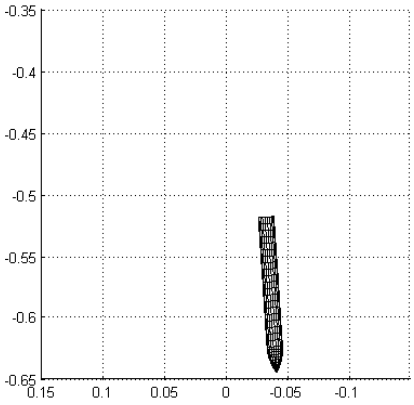

t = 1210 μs

Figure 6.

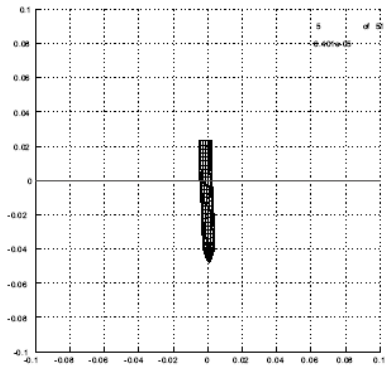

t = 64 μs

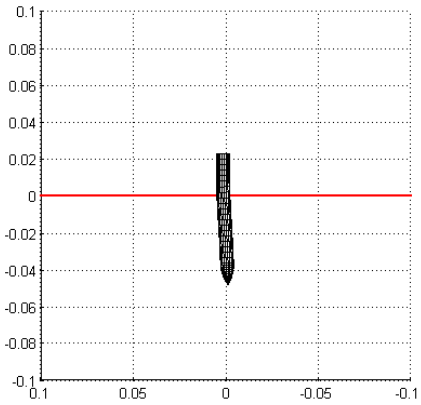

t = 65 μs

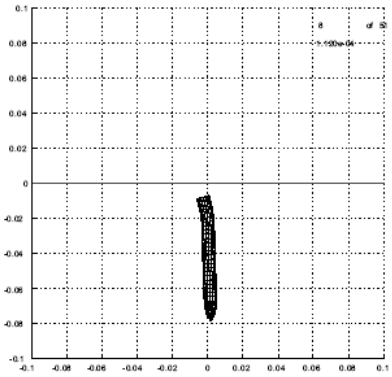

t = 112 μs

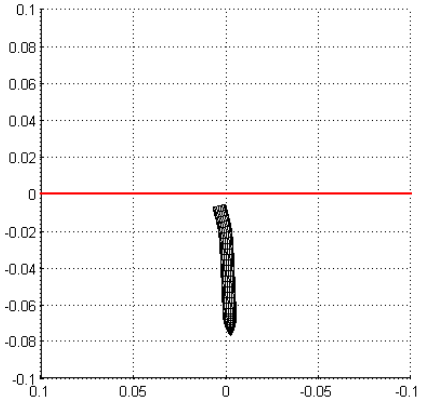

t = 110 μs

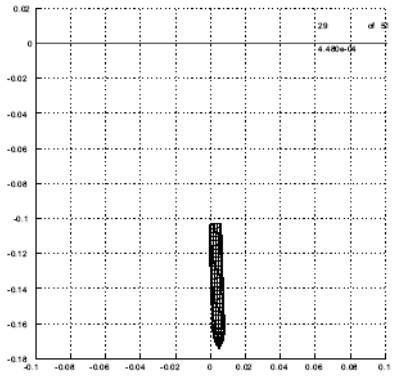

t = 448 μs

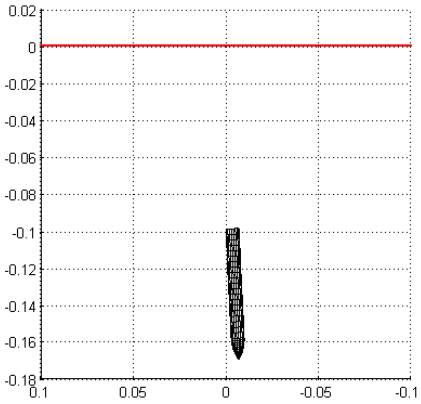

t = 450 μs

Figure 7.

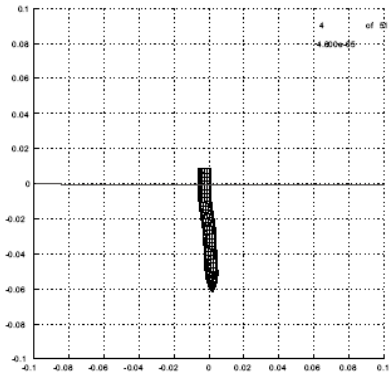

t = 48 μs

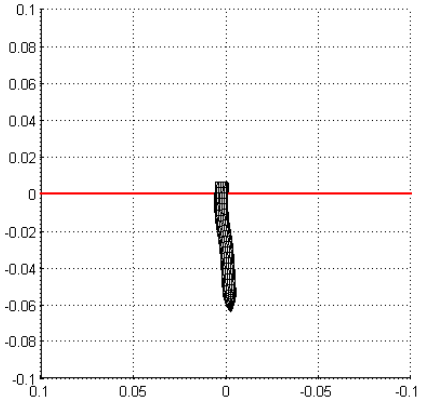

t = 50 μs

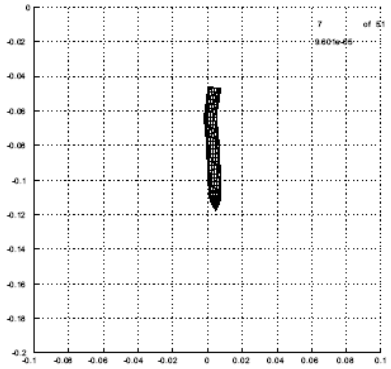

t = 96 μs

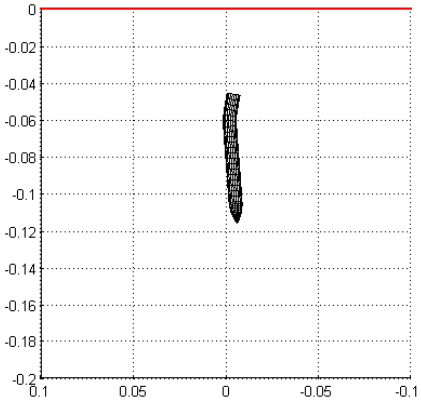

t = 95 μs

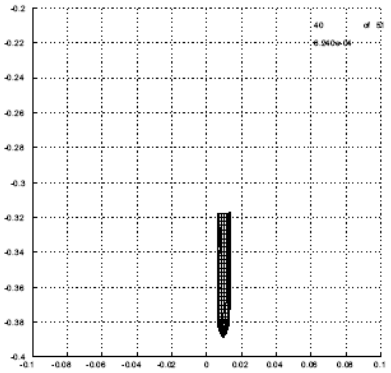

t = 624 μs

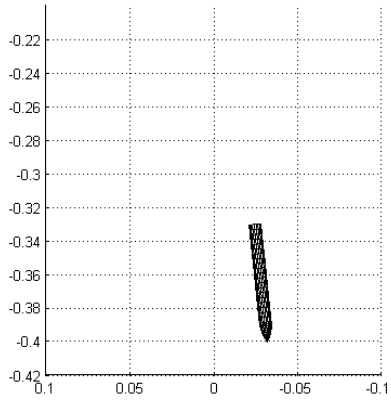

t = 625 μs

Figure 8.

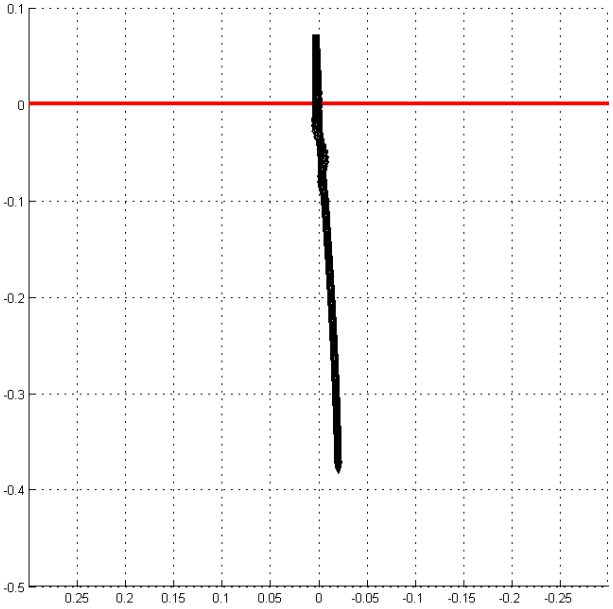

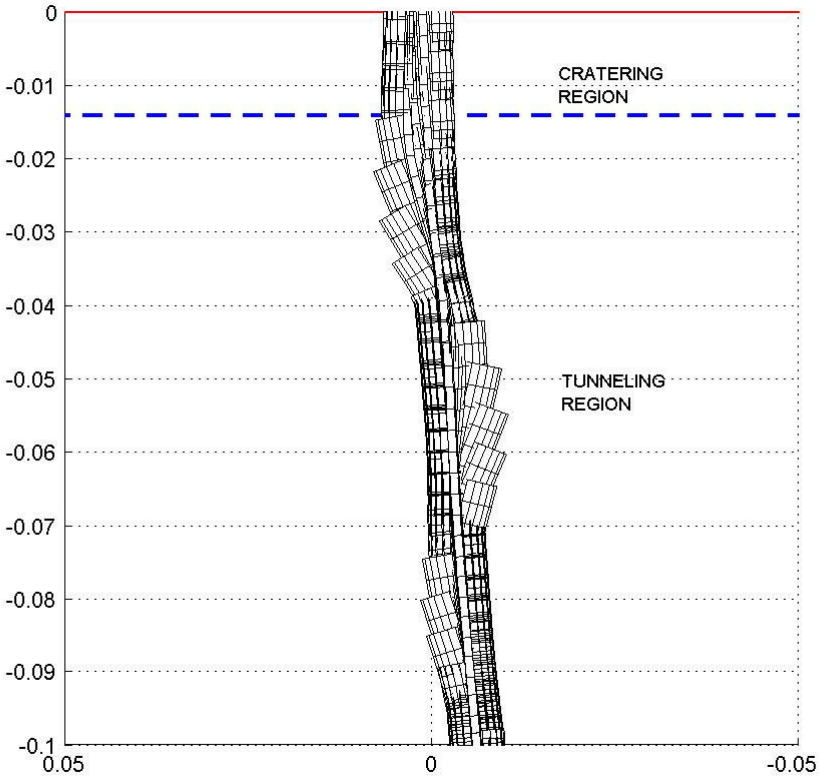

Figure 9.